10-2015

# Modeling NAPL Dissolution from Pendular Rings in Idealized Porous Media

Junqi Huang

John A. Christ

Mark N. Goltz
*Air Force Institute of Technology*

Avery H. Demond



## Recommended Citation

Huang, J., Christ, J. A., Goltz, M. N., & Demond, A. H. (2015). Modeling NAPL dissolution from pendular rings in idealized porous media. Water Resources Research, 51(10), 8182–8197. https://doi.org/10.1002/2015WR016924

AGU PUBLICATIONS

Water Resources Research

RESEARCH ARTICLE
10.1002/2015WR016924

# Modeling NAPL dissolution from pendular rings in idealized porous media

**Junqi Huang[1], John A. Christ[2], Mark N. Goltz[3], and Avery H. Demond[4]**

[1]Ground Water and Ecosystems Restoration Division, National Risk Management Research Laboratory, U.S. Environmental Protection Agency, Ada, Oklahoma, USA, [2]Department of Civil and Environmental Engineering, U.S. Air Force Academy, USAF Academy, Colorado, USA, [3]Department of Systems Engineering and Management, Air Force Institute of Technology, Wright-Patterson Air Force Base, Ohio, USA, [4]Department of Civil and Environmental Engineering, University of Michigan, Ann Arbor, Michigan, USA

**Key Points:**
- Exact solution to the Young-Laplace equation for pendular rings
- Theoretical determination of the mass transfer rate coefficient under hydrophobic conditions
- Predicts similar NAPL dissolution rates for oil-wet and water-wet conditions

**Correspondence to:**
J. Huang,
huang.junqi@epa.gov

**Citation:**
Huang, J., J. A. Christ, M. N. Goltz, and A. H. Demond (2015), Modeling NAPL dissolution from pendular rings in idealized porous media, *Water Resour. Res.*, *51*, 8182–8197, doi:10.1002/2015WR016924.

Received 13 JAN 2015
Accepted 7 SEP 2015
Accepted article online 21 SEP 2015
Published online 17 OCT 2015

**Abstract** The dissolution rate of nonaqueous phase liquid (NAPL) often governs the remediation time frame at subsurface hazardous waste sites. Most formulations for estimating this rate are empirical and assume that the NAPL is the nonwetting fluid. However, field evidence suggests that some waste sites might be organic wet. Thus, formulations that assume the NAPL is nonwetting may be inappropriate for estimating the rates of NAPL dissolution. An exact solution to the Young-Laplace equation, assuming NAPL resides as pendular rings around the contact points of porous media idealized as spherical particles in a hexagonal close packing arrangement, is presented in this work to provide a theoretical prediction for NAPL-water interfacial area. This analytic expression for interfacial area is then coupled with an exact solution to the advection-diffusion equation in a capillary tube assuming Hagen-Poiseuille flow to provide a theoretical means of calculating the mass transfer rate coefficient for dissolution at the NAPL-water interface in an organic-wet system. A comparison of the predictions from this theoretical model with predictions from empirically derived formulations from the literature for water-wet systems showed a consistent range of values for the mass transfer rate coefficient, despite the significant differences in model foundations (water wetting versus NAPL wetting, theoretical versus empirical). This finding implies that, under these system conditions, the important parameter is interfacial area, with a lesser role played by NAPL configuration.

## 1. Introduction

Nonaqueous phase liquid (NAPL) contamination at subsurface sites presents a persistent source of dissolved phase contamination, which can drive the site's remediation strategy and time to cleanup [*US EPA*, 2003; *Christ et al*., 2005]. When released, NAPL migrates downward to and often below the water table (depending on its density and the fluctuations of the water table) where it can become immobilized in discontinuous forms or in high saturation pools [*Mercer and Cohen*, 1990; *Kueper et al*., 1993]. The discontinuous forms may be single-pore or multipore blobs, or pendular rings depending on the porous media geometry and wettability characteristics. Although NAPLs are often assumed to be nonwetting relative to the aquifer solids, the partitioning and sorption of trace constituents in the NAPLs (e.g., surfactants, organic acids, and bases) can lead to organic-wetting conditions [*Powers and Tamblin*, 1995; *Lord et al*., 1997a, 1997b; *Zheng and Powers*, 1999; *Dwarakanath et al*., 2002; *Ryder and Demond*, 2008]. Soil systems containing complex NAPLs, such as coal tars and creosotes, are often organic wetting [*Hugaboom and Powers*, 2002; *Birak and Miller*, 2009]. If the system is organic wetting, the residual NAPL may be distributed as pendular rings surrounding the contact points of soil grains. In such scenarios, the dissolution of the NAPL from pendular rings can become a dominant factor in long-term site management.

The dissolution of the NAPL in the subsurface is a function of the interfacial area between the NAPL and aqueous phase, the concentration gradient that is the driving force for mass transfer from the NAPL surface to the bulk aqueous fluid, and the diffusion coefficient across the boundary layer [*Weber and DiGiano*, 1996]. A variety of studies have focused on different aspects of the dissolution process, including the influence of the aqueous and NAPL saturation geometry on interfacial mass transfer [*Knutson et al*., 2001; *Culligan et al*., 2004; *Cho and Annable*, 2005; *Brusseau et al*., 2006], the fitting of laboratory dissolution measurements to develop empirical models [*Miller et al*., 1990; *Imhoff et al*., 1994; *Powers et al*., 1994b], and the employment of pore-

scale models to delineate the influence of pore structure on the rate of mass exchange [*Reeves and Celia*, 1996; *Held and Celia*, 2001; *Dobson et al*., 2006]. These studies, however, generally assume that the porous medium is hydrophilic and that the NAPL configuration is in the form of spherical blobs immobilized in pore bodies [*Gvirtzman and Roberts*, 1991]. However, as *Dwarakanath et al*. [2002] point out, such assumptions ignore the field evidence of altered wettabilities at waste sites. The five systems contaminated with NAPL that *Dwarakanath et al*. [2002] investigated were mixed wet to oil wet; none were water wet. Thus, the dissolution of a wetting NAPL, distributed as pendular rings surrounding the contact points of soil grains, needs to be considered as a feasible scenario that may be encountered in the field.

The rate of dissolution depends on the interfacial area between the NAPL and the aqueous phase. *Reeves and Celia* [1996] presented a pore-scale network model that explored the relationship between capillary pressure ($P_c$), water saturation ($S_w$), and liquid-liquid (water ($w$)-NAPL ($n$)) specific interfacial area ($A_{nw}$). The network model conceptualized the porous medium as a cubic lattice (pore bodies) connected by uniformly distributed biconical tubes, which allowed a direct computation of the interfacial geometry including the radius of the pore throat menisci. Simulation results demonstrated a well-behaved $P_c$-$S_w$-$A_{nw}$ relationship [*Hassanizadeh and Gray*, 1993], implying that direct estimates of $A_{nw}$ could be obtained from the $P_c$-$S_w$ relationship. Based on the earlier work of *Hassanizadeh and Gray* [1993], *Held and Celia* [2001] developed a computational pore-scale model that included mass transfer and explicitly tracked the liquid-liquid interfaces, enabling a more accurate investigation of local and effective mass transfer coefficients. Furthermore, by including nonwetting phase snap-off and retraction of NAPL from the pore body to the pore throats, they more closely simulated conditions that may be present in systems with a significant quantity of NAPL immobilized as pendular rings. A thermodynamically based model for predicting two-fluid interfacial area within a porous medium as a function of fluid phase saturation and saturation history was presented by *Grant and Gerhard* [2007], which is an extension of the thermodynamic model developed by *Leverett* [1941]. More recently, *Porter et al*. [2010] used thermodynamic considerations which suggested that $A_{nw}$ is proportional to the work of fluid displacement as estimated by the area under the $P_c$-$S_w$ curve [*Leverett*, 1941] to examine the dependence of $A_{nw}$ on $S_w$. However, these thermodynamically based approaches estimated the NAPL-aqueous phase specific surface area indirectly and, therefore, did not require knowledge of the NAPL morphology.

More recent work has continued to refine these pore-scale approaches. For example, *Bear et al*. [2011] analyzed the analytical solutions to the Young-Laplace equation presented by *Melrose* [1966] and *Orr et al*. [1975] using a geometrical approach and idealized wetting-nonwetting interfacial morphologies (e.g., nodoid, catenoid, negative unduloid, cylinder, positive unduloid, sphere, and positive nodoid). However, their work elucidated the influence of morphology on the $P_c$-$S_w$ relationship, not on interfacial area. The work of *Rubinstein and Fel* [2013] concentrated on the topology of pendular rings bridging two solid surfaces and derived an elegant set of equations in parametric form for the curvature, volume, and surface area as a function of the fluid filling angle. However, they did not attempt to apply these equations to the phenomenon of pendular ring dissolution.

This work focuses specifically on modeling the dissolution from NAPL distributed as pendular rings in the subsurface in organic-wetting systems. A set of novel, exact solutions to the Young-Laplace equation for a porous medium idealized as spherical particles in a hexagonal close packing was developed to quantify the pendular ring surface area and volume as a function of the NAPL saturation. Volume averaging yielded macroscopic quantities for NAPL saturation and interfacial area per unit volume of the porous medium, which when coupled with a pore-scale transport model based on Hagen-Poiseuille flow in a capillary tube, gave a rate coefficient quantifying mass transfer from the NAPL to the aqueous phase. Regression functions were also developed to enable simpler calculations of the NAPL dissolution rate coefficient based on the analytic solutions for the pendular ring interfacial area and the diffusive flux across the NAPL-water interface in a capillary tube. This new function employs the NAPL saturation, solid particle radius, and contact angle as well as a modified Peclet number to estimate the mass transfer rate coefficient for NAPL dissolution.

## 2. Model Development

### 2.1. Pendular Ring Surface

Quantifying NAPL dissolution requires a specification of the interfacial area between the NAPL ($n$) and the aqueous ($w$) phases. Here the porous medium is idealized as spheres arranged in a hexagonal

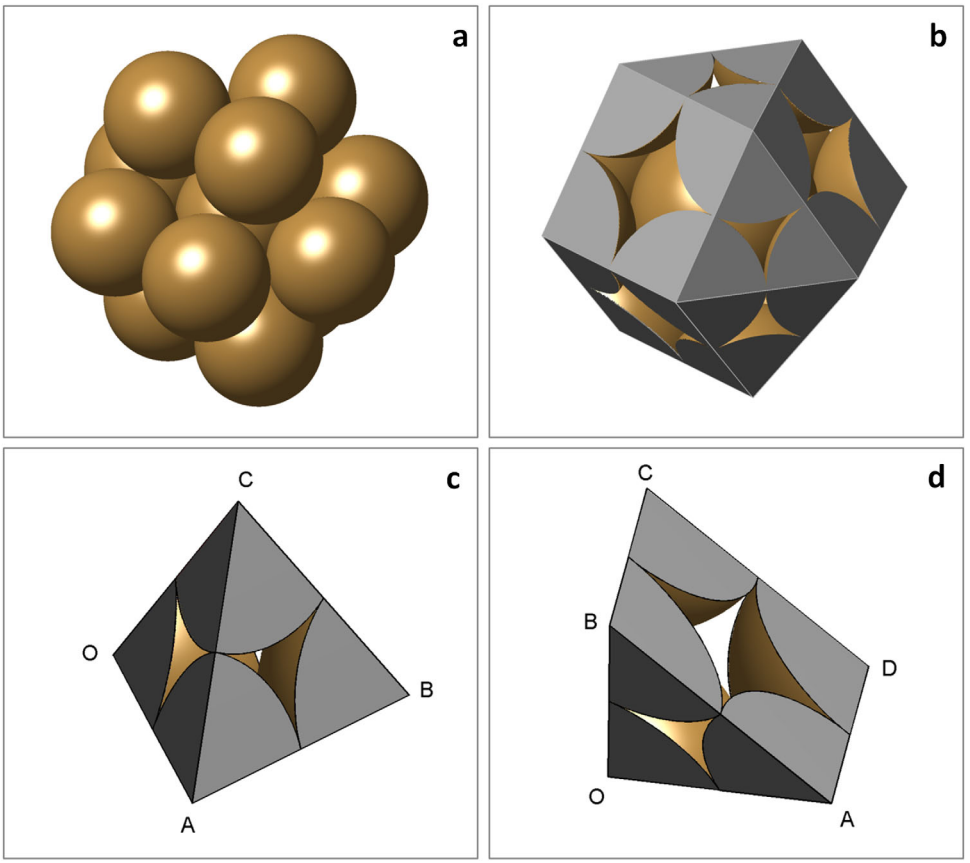


**Figure 1.** (a) Closed hexagonal packing cluster containing 13 spheres (coordination number = 12), (b) a triangular orthobicupola comprising a hexagonal unit cell, made up of (c) regular tetrahedrons containing sections of four spheres and (d) square pyramids containing sections of five spheres.

close packing, which has a coordination number of 12 (Figure 1a). Figure 1b depicts the hexagonal unit cell surrounding the center spherical particle. This unit cell is composed of eight regular tetrahedrons (Figure 1c) and six square pyramids (Figure 1d), which dictate the shape and volume of the residual NAPL.

It is assumed that the residual NAPL resides as the wetting fluid distributed as pendular rings surrounding the contact point between two soil particles (Figure 2a). The shape of a pendular ring surrounding the contact point between two spheres can be described by the Young-Laplace equation as [*Rey*, 2000]:

$$\sigma \nabla \cdot \hat{\mathbf{n}} = -\Delta p \tag{1}$$

where $\hat{\mathbf{n}}$ is the outward unit normal vector for the pendular ring surface, $\sigma$ is the NAPL-water interfacial tension, and $\Delta p$ is the pressure difference ($p_{NAPL} - p_{water}$) across the interface due to the surface curvature. The general solution to (1) in a three-dimensional space has the form $f(x, y, z) = 0$ and the outward unit normal vector for this surface may be written as:

$$\hat{\mathbf{n}} = \frac{f_x \hat{\mathbf{x}} + f_y \hat{\mathbf{y}} + f_z \hat{\mathbf{z}}}{\sqrt{f_x^2 + f_y^2 + f_z^2}} \tag{2}$$

where $f_x = \partial f / \partial x$, $f_y = \partial f / \partial y$, $f_z = \partial f / \partial z$, and ($\hat{\mathbf{x}}$, $\hat{\mathbf{y}}$, $\hat{\mathbf{z}}$) are the unit vectors in Cartesian space.

However, given that the pendular ring resides at the contact point between two soil particles and is generally assumed to have a surface symmetric about a line connecting the centers of these two particles (Figures 2b and 2c), the surface is more readily described in cylindrical coordinates as a function $r = f(z)$, which upon substitution into equation (1) yields:

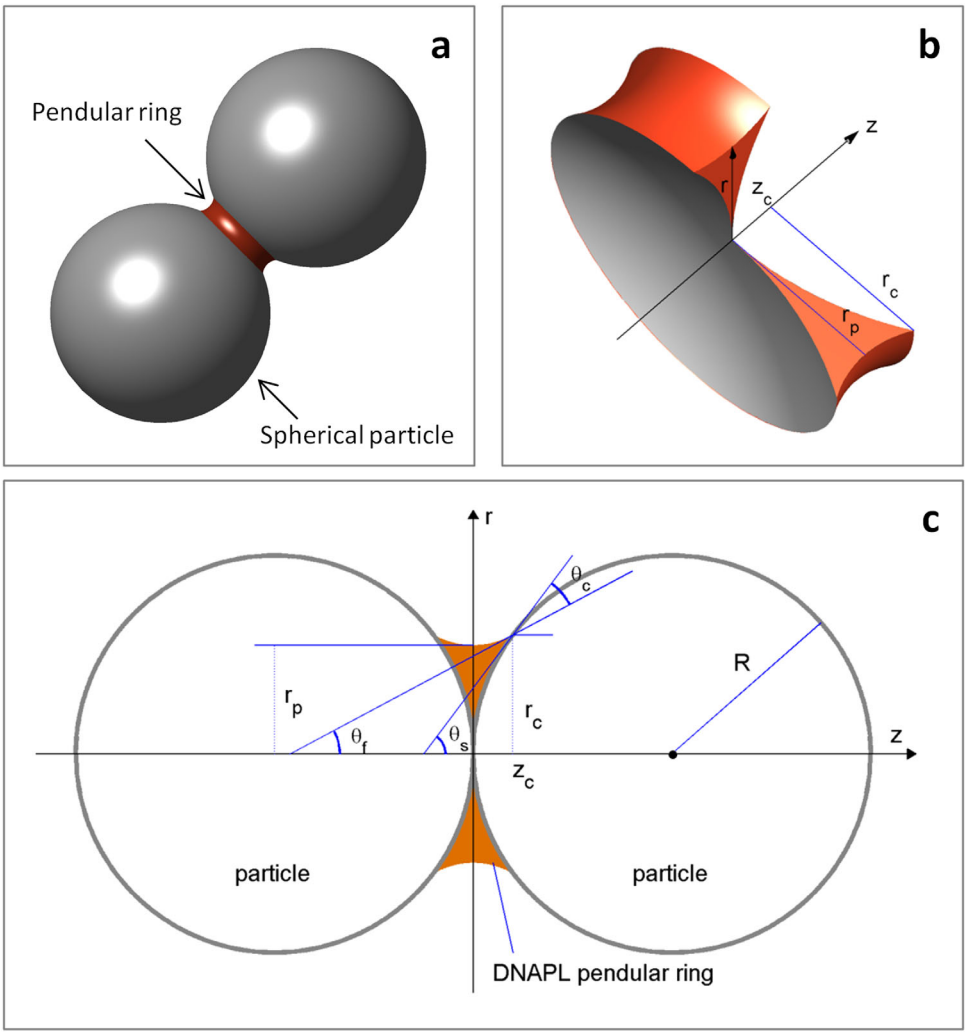


**Figure 2.** (a) Pendular ring at the contact point between two spherical particles, (b) cross section of a pendular ring cut along the *r* direction, (c) pendular ring in two-dimensional cylinder coordinates. Note that the actual shape of a pendular ring in three dimensions is the object generated by revolving about the *z* axis as shown in Figure 2b.

$$\frac{1}{r(1+r'^2)^{1/2}}-\frac{r''}{(1+r'^2)^{3/2}}=\frac{\Delta p}{\sigma} \tag{3}$$

where $r'=\partial f/\partial z$ and $r''=\partial^2 f/\partial z^2$. Figure 2c shows that the pendular ring radius ($r$) ranges from $r=r_p$ to $r=r_c$, where $r_p$ is the radius of the pendular ring at $z=0$, and $r_c$ is the radius of the pendular ring at $z=z_c$, i.e., where the pendular ring contacts the surface of the spherical particle with a contact angle $\theta_c$, measured through the NAPL. This contact angle is an experimentally quantifiable thermodynamic property, and is assumed to be known and single valued for a specific solid-liquid-liquid combination. These two constraints on the pendular ring surface:

$$r=r_p,\ z=0 \tag{4a}$$

$$\frac{\partial r}{\partial z}=\tan(\theta_f),\ z=z_c \tag{4b}$$

where $\theta_f$ is the angle between the $z$ axis and the line tangent to the pendular ring surface passing through the point ($z_c$, $r_c$) (as shown in Figure 2c), provide the boundary conditions necessary for the solution of equation (3). To facilitate the solution of equation (3) subject to equations (4a) and (4b), equation (3) was transformed to:

$$\frac{1}{rr'}\frac{\partial}{\partial z}\left[\frac{r}{(1+r'^2)^{1/2}}\right]=2k \tag{5}$$

where $k=\Delta p/(2\sigma)$. Equation (5) can be readily integrated to give:

$$\frac{r}{(1+r'^2)^{1/2}}=kr^2+F \tag{6}$$

where $F$ is the integration constant, which is determined by applying the boundary condition equation (4b):

$$F=\frac{r_c}{[1+\tan^2(\theta_f)]^{1/2}}-kr_c^2 \tag{7a}$$

Given that $\theta_f=\theta_s-\theta_c$ (where $\theta_s$ is the angle between the $z$ axis and the line tangent to the sphere surface passing through the point ($z_c$, $r_c$), as defined in Figure 2c):

$$\tan(\theta_f)=\frac{\tan(\theta_s)-\tan(\theta_c)}{1+\tan(\theta_s)\tan(\theta_c)} \tag{7b}$$

based on the angle addition formula for the tangent function. Furthermore, $\tan(\theta_s)$ is the slope of the line tangent to the sphere surface at $r=r_c$, which can be represented by:

$$\tan(\theta_s)=\frac{1}{r_c}\sqrt{R^2-r_c^2} \tag{7c}$$

where $R$ is the radius of the spherical particles. Employing equations (7b) and (7c), the integration constant $F$ may be rewritten as:

$$F=\frac{r_c}{R}[r_c\cos(\theta_c)+\sqrt{R^2-r_c^2}\sin(\theta_c)]-kr_c^2 \tag{7d}$$

Thus, the solution to equation (6), using the form of the integration constant presented in equation (7d), is:

$$\int_{r_c}^{r}\frac{kr^2+F}{[r^2-(kr^2+F)^2]^{1/2}}dr=z+B \tag{8}$$

where $B$ is the second integration constant that can be determined using the boundary condition given in equation (4a):

$$B=\int_{r_c}^{r_p}\frac{kr^2+F}{[r^2-(kr^2+F)^2]^{1/2}}dr \tag{9}$$

with $r_p$ still unknown. However, based on the pendular ring symmetry in the $r$-$z$ plane, it is clear that an extrema must be present at $z=0$ and $r=r_p$; thus, $r'=0$ at this location. Applying these conditions to equation (6), the parameter $r_p$ is obtained by finding the roots of:

$$kr_p^2-r_p+F=0 \tag{10a}$$

giving:

$$r_p=\frac{1}{2k}(1\pm\sqrt{1-4kF}) \tag{10b}$$

The root selection for equation (10b) is determined by $r_p < r_c$ as the NAPL is assumed to be the wetting phase.

Thus, assuming $k$ can be determined, the solution describing the surface of a NAPL pendular ring at the interface connecting two solid spheres in $r$-$z$ space is:

$$z=\int_{r_c}^{r}\frac{kr^2+F}{[r^2-(kr^2+F)^2]^{1/2}}dr-B \tag{11}$$

Equation (11) involves three prescribed parameters: $R$, $\theta_c$, and $r_c$, and one parameter that needs to be determined, $k$. The parameter $k$ has been shown to be the eigenvalue of equation (5) [*Rubinstein and Fel*, 2013], which can be determined separately based on additional boundary conditions.

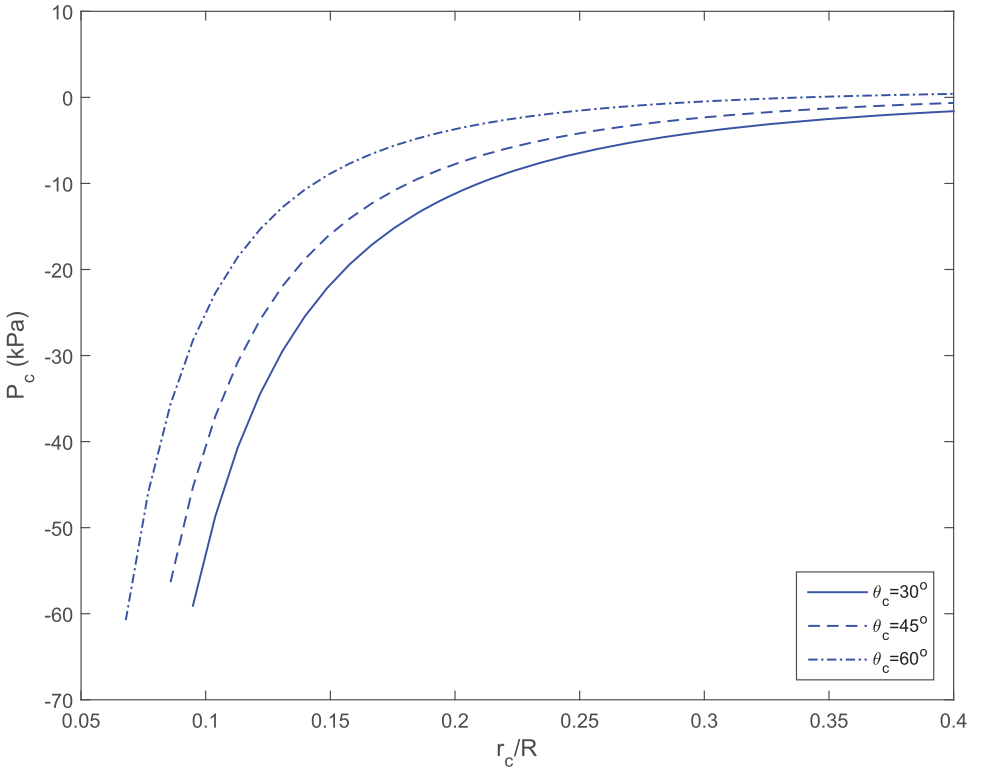


**Figure 3.** Capillary pressure ($p_{NAPL}-p_{water}$) as a function of pendular ring radius at the contact point ($r_c$) normalized to the solid particle radius ($R$) for three different contact angles: $\theta_c=30^\circ$, $\theta_c=45^\circ$, and $\theta_c=60^\circ$. $r_c$ is a surrogate for NAPL saturation.

### 2.2. Capillary Pressure-Saturation Relationship

Recognizing that the pressure difference across the pendular ring surface, $\Delta p=p_{NAPL}-p_{water}$ commonly referred to as the capillary pressure $p_c$, is given by $\Delta p=2\sigma k$, $k$ can be determined by noting that when $r=r_c$ in equation (11), $z_c=-B$, and because $z=z_c$ lies on the surface of the spherical particle:

$$z_c=R-\sqrt{R^2-r_c^2} \tag{12}$$

Combining equations (9) and (12) gives:

$$\int_{r_c}^{r_p}\frac{kr^2+F}{\left[r^2-(kr^2+F)^2\right]^{1/2}}dr+R-\sqrt{R^2-r_c^2}=0 \tag{13}$$

Equation (13) is an important condition that can be used to find a unique value for $k$ that solves equation (3), assuming that $R$, $\theta_c$, and $r_c$ are known. Once $k$ is known, the capillary pressure can be calculated. *Rubinstein and Fel* [2013] demonstrated that for some combinations of $R$, $\theta_c$, and $r_c$, the eigenvalue $k$ does not exist. However, when $k$ does exist as a solution to equation (13), this equation represents a theoretical relationship between capillary pressure and saturation, as $r_c$ is a surrogate for NAPL saturation. Figure 3 displays the solution to equation (13) in terms of $p_c$ as a function of the pendular ring radius for several values of the contact angle $\theta_c$.

### 2.3. Pendular Ring Interfacial Area and Volume

To describe the surface of the pendular ring, which can then be used to find the interfacial area between the NAPL and water, equation (13) is first solved to obtain $k$, which is then used to solve equation (11). Equation (11) actually describes a curve. To obtain the pendular ring surface, this curve must be revolved

**Table 1.** Geometric Properties of a Regular Tetrahedron and a Square Pyramid[a]

| Property | Regular Tetrahedron | Square Pyramid |
|---|---|---|
| Volume | $V_T=\frac{1}{3}\sqrt{8}R^3$ | $V_P=\frac{1}{3}\sqrt{32}R^3$ |
| Solid angle | $\Omega_T=3\arccos(1/3)-\pi$ | $\Omega_P=4\arctan(\sqrt{2}/4)$ |
| Face edge face angle | $\varphi_T^{ff}=\arccos(1/3)$ | $\varphi_P^{ff}=\arccos(-1/3)$ |
| Face edge base angle | | $\varphi_P^{fb}=\arctan(\sqrt{2})$ |
| Volume occupied by solid | $V_T^s=\frac{4}{3}\Omega_T R^3$ | $V_P^s=\Omega_P R^3$ |
| Surface area of sphere | $S_T=4\Omega_T R^2$ | $S_P=3\Omega_P R^2$ |
| Number of pendular rings | $N_T=\frac{3}{\pi}\varphi_T^{ff}$ | $N_P=\frac{2}{\pi}(\varphi_P^{ff}+\varphi_P^{fb})$ |
| Number in a unit cell | 8 | 6 |

[a]R = radius of the spheres making up the porous medium.

around the $z$ axis, as shown in Figure 2b. The volume of the pendular ring ($V_{PR}$) can thus be obtained by integration:

$$V_{PR}=2\int_0^{z_c}\pi\{r^2-[R^2-(z-R)^2]\}dz \quad (14)$$

which, using equation (11), can be rewritten as:

$$V_{PR}=2\pi\int_{r_p}^{r_c}\frac{r^2(kr^2+F)}{\left[r^2-(kr^2+F)^2\right]^{1/2}}dr -2\pi\left[R^2z_c-\frac{1}{3}(z_c-R)^3-\frac{1}{3}R^3\right] \quad (15)$$

Likewise, the interfacial area between the NAPL and the aqueous phase, which is equivalent to the surface area of the NAPL pendular ring ($A_{PR}$), can be obtained by evaluating the integral:

$$A_{PR}=2\int_0^{z_c}2\pi r(1+r'^2)^{1/2}dz \quad (16)$$

which, using equation (11), can be rewritten as:

$$A_{PR}=4\pi\int_{r_p}^{r_c}\frac{r^2}{\left[r^2-(kr^2+F)^2\right]^{1/2}}dr \quad (17)$$

Equations (15) and (17) provide a means for quantifying the NAPL saturation and specific interfacial area, respectively. Given the volume and interfacial area of a single pendular ring and the geometry of the pore network, the individual volumes and areas can be summed to obtain an overall NAPL saturation and interfacial area. Based on Figure 1, there are eight regular tetrahedrons and six square pyramids in a unit cell that need to be summed over to obtain the overall unit cell behavior. Tables 1 and 2 give the formulas for computing the geometric quantities related to regular tetrahedrons and square pyramids. Once computed, they can be used to quantify the NAPL saturation, $S_n$, and specific interfacial area, $A_{nw}$, according to:

$$S_n=\frac{V_{NAPL}}{V_U-V_S}=\frac{18(2\varphi_T^{ff}+\varphi_P^{ff}+\varphi_P^{fb})}{20\sqrt{2}-(16\Omega_T+9\Omega_P)}\frac{V_{PR}}{\pi R^3} \quad (18)$$

$$A_{nw}=\frac{A_{NAPL}}{V_U}=\frac{9(2\varphi_T^{ff}+\varphi_P^{ff}+\varphi_P^{fb})}{10\sqrt{2}}\frac{A_{PR}}{\pi R^3} \quad (19)$$

(For the definitions of the variables in equations (18) and (19), see Tables 1 and 2.) Figure 4 depicts the specific interfacial area, $A_{nw}$ given by equation (19), as a function of the NAPL saturation, given by equation (18), for various solid particle radius ($R$) and contact angle ($\theta_c$) combinations. The range of values of NAPL saturation are typical of values found in the field [*Kueper et al.*, 1993; *Young et al.*, 1999] and are especially relevant during the latter part of a NAPL source remediation. The calculations show that as $R$ decreases, $A_{nw}$ increases regardless of the value of the contact angle; thus, a smaller particle size implies a larger area of contact between the NAPL and water, and higher rates of interphase mass transfer. Such a dependence has been demonstrated previously [*Cho and Annable*, 2005; *Dobson et al.*, 2006; *Brusseau et al.*, 2008].

**Table 2.** Unit Cell Geometric Properties[a]

| Parameter | Equation |
|---|---|
| Total volume ($V_U$) | $\frac{40\sqrt{2}}{3}R^3$ |
| Total volume of the solid ($V_S$) | $(\frac{32}{3}\Omega_T+6\Omega_P)R^3$ |
| Porosity ($\theta$) | $1-\frac{1}{20\sqrt{2}}(16\Omega_T+9\Omega_P)$ |
| Total volume of the NAPL ($V_{NAPL}$) | $\frac{12}{\pi}(2\varphi_T^{ff}+\varphi_P^{ff}+\varphi_P^{fb})V_{PR}$ |
| Total surface of the NAPL ($A_{NAPL}$) | $\frac{12}{\pi}(2\varphi_T^{ff}+\varphi_P^{ff}+\varphi_P^{fb})A_{PR}$ |

[a]$R$ = radius of the spheres making up the porous medium. $V_{PR}$ is given by equation (15); $A_{PR}$ is given by equation (17).

### 2.4. Mass Transfer Rate Coefficient

The function describing the specific surface area of pendular rings derived in the previous section can form the basis for a theoretical quantification of NAPL dissolution from pendular rings. Since the interphase mass transfer is a function of the

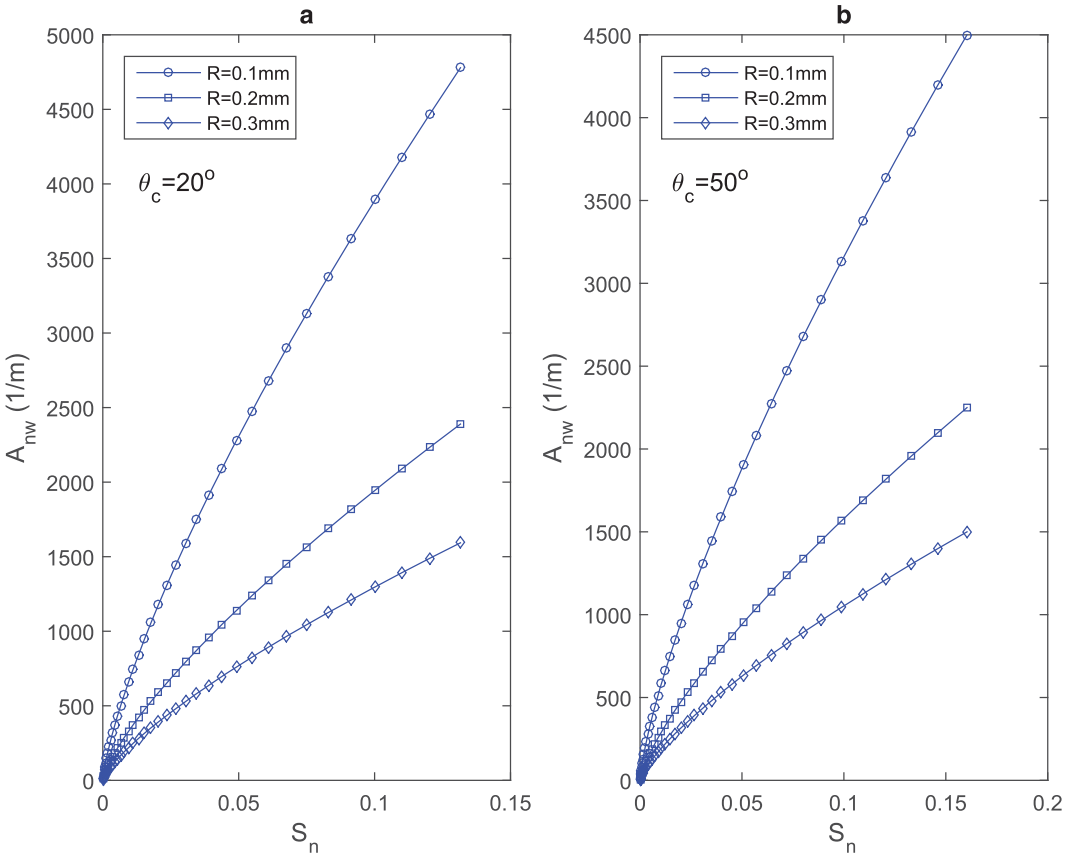


**Figure 4.** Specific interfacial area between the NAPL and the aqueous phase as a function of NAPL saturation for various particle radii ($R$) assuming (a) $\theta_c=20^\circ$ and (b) $\theta_c=50^\circ$.

interfacial area where the dissolution is occurring, the interfacial area must also be incorporated in the expression of the rate of dissolution [*Powers et al*., 1994a]. The rate of mass transport, $N_d$, may be given as [*Miller et al*., 1990; *Held and Celia*, 2001]:

$$N_d=A_{nw}D_m\frac{\partial C}{\partial \hat{n}}=A_{nw}k_l(C_s-C_i) \tag{20}$$

where $A_{nw}$ is the specific surface area of NAPL, $D_m$ is the bulk aqueous phase diffusion coefficient of the solute, $C$ is the local aqueous concentration of NAPL associated with the NAPL surface, $\hat{n}$ is the normal vector of the interface between water and NAPL, $C_s$ is the aqueous phase solubility of NAPL, $C_i$ is the bulk aqueous phase concentration of NAPL, and $k_l$ is the mass transfer coefficient. Investigators who have used a linear difference in concentration as the driving force for NAPL dissolution have typically lumped $A_{nw}$ and $k_l$ together to define a mass transfer rate coefficient $\alpha$, where $\alpha=A_{nw}k_l$, so that the mass transfer coefficient and the specific interfacial area do not need to be determined independently [*Miller et al*., 1990; *Imhoff et al*., 1994; *Powers et al*., 1994a].

Yet to obtain deeper insight into the process of NAPL dissolution, it is necessary to independently quantify the mass transfer coefficient and specific surface area appearing in equation (20). In the previous section, we derived a theoretical expression for the specific surface area $A_{nw}$; here we quantify the mass transfer coefficient $k_l$. The task of obtaining an analytical expression for $k_l$ is not trivial since the parameter depends on several factors including fluid velocity, pore size, and solute diffusivity. As suggested by equation (20), the mass transfer coefficient may be mathematically represented as:

$$k_l=D_m\frac{\partial C}{\partial \hat{n}}\frac{1}{(C_s-C_i)} \tag{21}$$

To generate an analytic expression for $k_l$, it is assumed that the porous medium can be represented as a bundle of capillary tubes with the equivalent pore radius, $R_c$, and porosity, $\theta$, of the hexagonal unit cell, as conceptualized in Figure A1. Then, using the approach developed in Appendix A, the mass transfer coefficient can be written as:

$$k_l = \frac{D_m}{R_c} f(Pe') \tag{22}$$

where

$$f(Pe') = \left[ 2a' \frac{M(a'+1, 2, i\sqrt{Pe'})}{M(a', 1, i\sqrt{Pe'})} - 1 \right] i\sqrt{Pe'} \tag{23}$$

$$a' = \left( \frac{1}{2} - i\frac{1}{4}\sqrt{Pe'} \right) \tag{24}$$

$$Pe' = \frac{2vR_c^2}{D_m \Delta x} \tag{25}$$

$$R_c = \frac{40\sqrt{2}}{48\Omega_T + 27\Omega_P} \theta R \tag{26}$$

$$\Delta x = \frac{[60\sqrt{2} - 3(16\Omega_T + 9\Omega_P)](16\Omega_T + 9\Omega_P)^2}{22400\pi} \frac{R}{\theta^2} \tag{27}$$

and $M(\cdots)$ is the Kummer's function of the first kind, $v$ is the average pore fluid velocity, $\Delta x$ is the characteristic length over which the dissolution occurs, $\Omega_T$ and $\Omega_P$ are the solid angle of a regular tetrahedron and a square pyramid, respectively (Table 1), and $i = \sqrt{-1}$. Using equation (22), equation (20) becomes:

$$N_d = A_{nw} \frac{D_m}{R_c} f(Pe')(C_s - C_i) \tag{28}$$

Thus, the mass transfer rate coefficient, $\alpha$, can be calculated as:

$$\alpha = A_{nw} \frac{D_m}{R_c} f(Pe') \tag{29}$$

### 2.5. Simplification of Theoretical Model for Calculation of Mass Transfer Rate Coefficient

Using equation (29) to find the mass transfer rate coefficient requires determining the parameters $A_{nw}$, which requires solving the Young-Laplace equation, and the function $f(Pe')$, which requires evaluating a Kummer's function [*Pearson*, 2009]. Hence, simpler relationships for calculating the interfacial area and the function $f(Pe')$ would be useful for general calculations. The theoretical analysis of the pendular ring undertaken here revealed that the relationship between $A_{nw}$ and $\theta_c$ describes a caternary curve and thus can be described by a hyperbolic cosine function (cos*h*). Furthermore, if $\theta_c$ approaches 90°, the curve describing the pendular ring has a minimum curvature (and thus a minimum area), suggesting that a factor of $\theta_c - \pi/2$ may be appropriate. Performing a series of regression analyses using MATLAB's least squares fitting routine between the solid particle radius $R$, NAPL contact angle $\theta_c$, and NAPL saturation $S_n$ as the independent variables, and calculated values of $A_{nw}$ obtained by solving equation (19) as the dependent variable, yielded:

$$A_{nw} = \frac{\lambda \cosh(2\theta_c/\pi - 1)}{R} S_n^{\beta} \tag{30}$$

where $\lambda = 1.604$ and $\beta = 0.746$ are the best fit values.

The function $f(Pe')$ is univariate with only a single independent variable, $Pe'$. Interestingly, the function $f(Pe')$ appears to possess different forms for $0 \leq Pe' \leq 1$ and $Pe' > 1$, and thus is perhaps better fitted with two different power functions. Performing a series of regression analyses fitting $f(Pe')$ as the dependent variable yielded:

$$f = \begin{cases} k_1 (Pe')^{\gamma_1}, & 0 \leq Pe' \leq 1 \\ k_2 (Pe')^{\gamma_2} + d_2, & Pe' > 1 \end{cases} \tag{31}$$

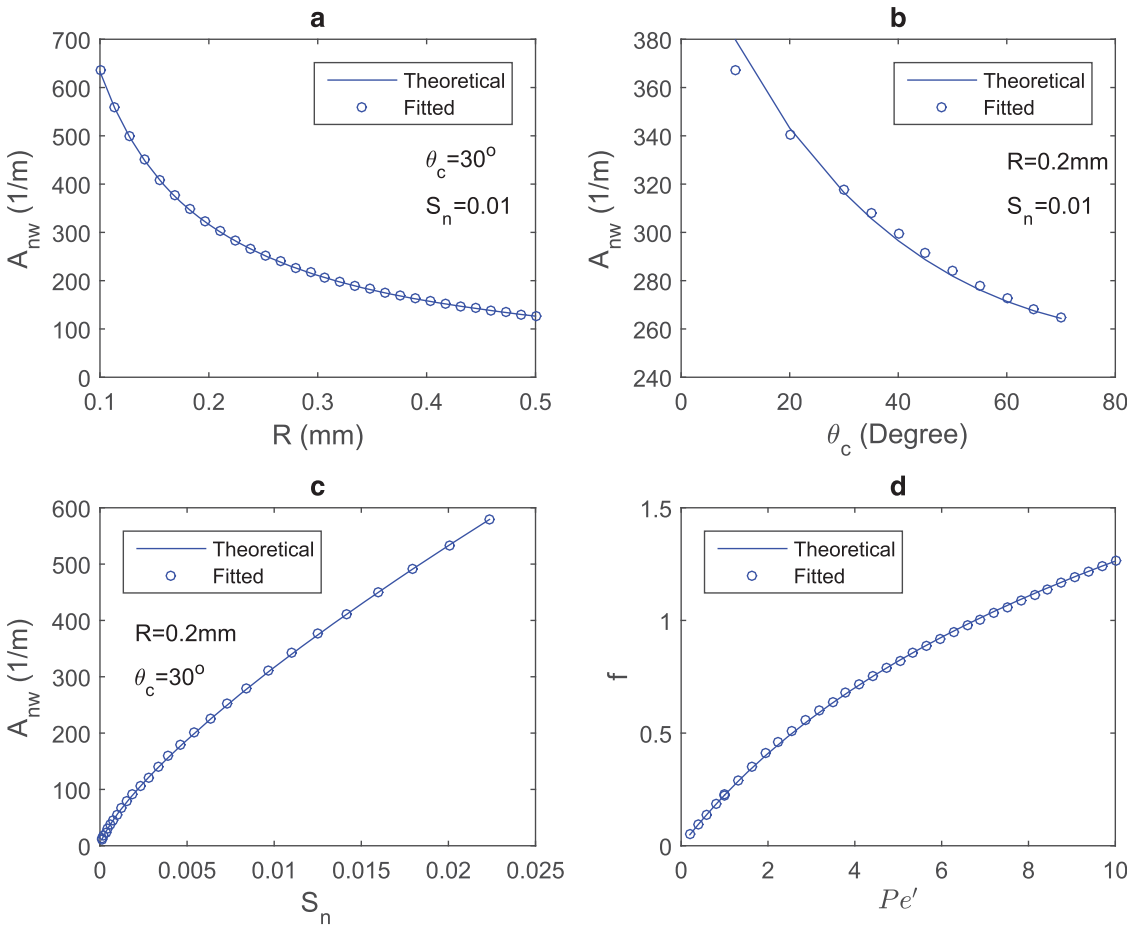


**Figure 5.** Comparison between calculations of the NAPL specific surface area ($A_{nw}$) using equation (19) (solid line) and equation (30) (symbols) as a function of (a) particle radius ($R$), (b) contact angle ($\theta_c$), and (c) NAPL saturation ($S_n$). (d) Comparison between the calculation of the function $f(Pe')$ using equation (23) (solid line) and equation (31).

where $k_1=0.227$, $\gamma_1=0.948$, $k_2=0.482$, $\gamma_2=0.500$, and $d_2=-0.260$ are the best fit values. Figures 5a–5c compare the values of the specific surface area of the NAPL calculated using equation (30) (fitted) and equation (19) (theoretically calculated), whereas Figure 5d shows $f(Pe')$ calculated using equation (31) (fitted) and equation (23) (theoretically calculated). The goodness of fit between the fitted and calculated values shown in this figure suggests that there is a minimal loss of accuracy in using the equations found by regression, particularly if the contact angle is $20^\circ \le \theta_c \le 70^\circ$.

Using the simplified forms for $A_{nw}$ (equation (30)) and $f(Pe')$ (equation (31)), the mass transfer rate coefficient may be written as:

$$\alpha = \frac{7.0 D_m}{R^2}\cosh(2\theta_c/\pi - 1) S_n^{0.746} \begin{cases} 0.227(Pe')^{0.948}, & 0 \le Pe' \le 1 \\ 0.482(Pe')^{1/2} - 0.260, & Pe' > 1 \end{cases} \tag{32}$$

## 3. Comparison of Theoretical Model to Other Formulations

Conventionally, a modified Sherwood number defined as $Sh' = \alpha d_{50}^2 / D_m$ [e.g., *Miller et al.*, 1990; *Powers et al.*, 1994a] can be used to calculate the mass transfer rate coefficient. Based on the formulation for $\alpha$ presented in equation (29):

$$Sh' = \frac{4R^2 A_{nw}}{R_c} f(Pe') \tag{33}$$

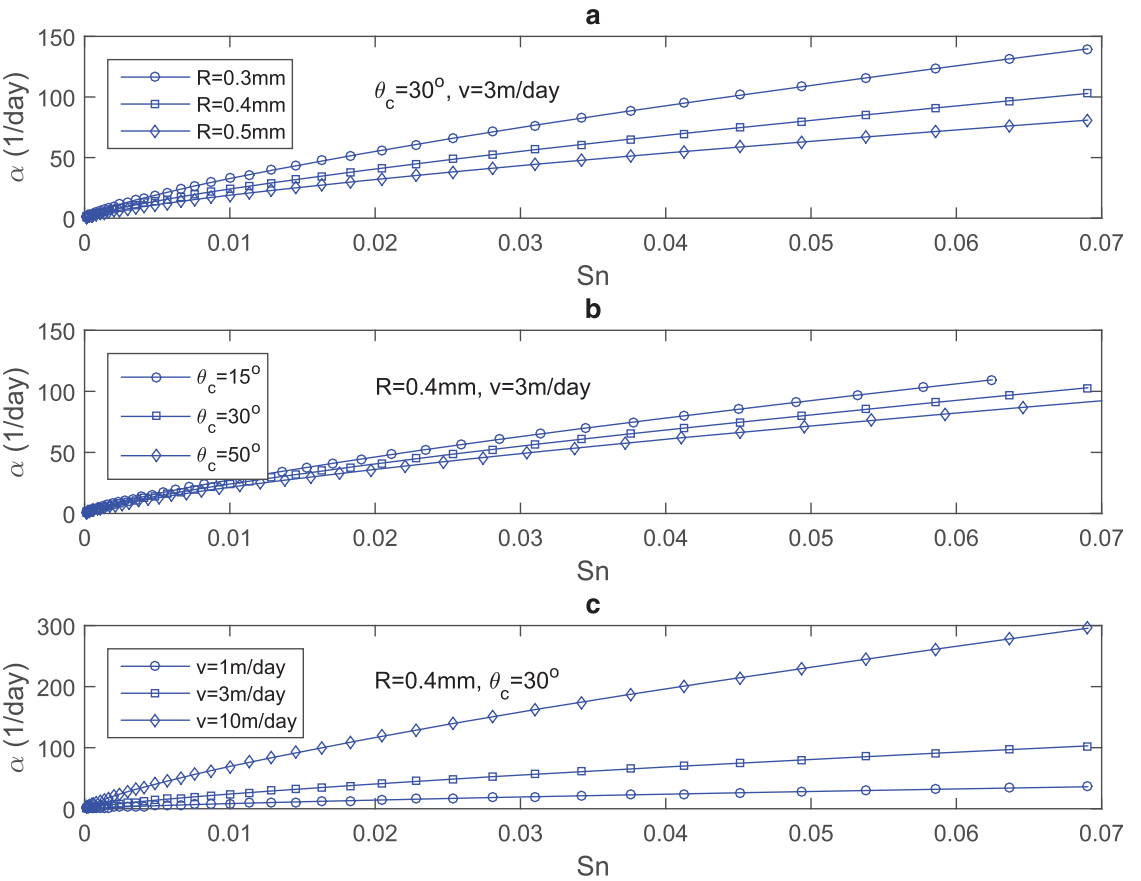


**Figure 6.** Mass transfer rate coefficient (in units of days$^{-1}$) as a function of NAPL saturation for (a) different solid particle radii, assuming a contact angle of 30° and an average fluid pore velocity of 3 m/d, (b) different contact angles assuming a solid particle radius of 0.4 mm and an average fluid pore velocity of 3 m/d, and (c) different average fluid pore velocities assuming a solid particle radius of 0.4 mm and a contact angle of 30°.

The form of the Sherwood number given in equation (33) is consistent with those derived using experimental studies and empirical models, yet has the advantage of providing a theoretical basis for the rate of mass transfer that can be evaluated explicitly to show the dependence of $\alpha$ on $S_n$, $v$, $R$, and $\theta_c$ for an organic-wetting system. For example, if $S_n$=0.005, $v$=3 m/d, $R$=0.4 mm, and $\theta_c$=30°, $\alpha$ equals 14.33 1/day (Figure 6a). Figure 6a illustrates that as the NAPL saturation increases, the mass transfer rate coefficient increases due to the coincident increase in interfacial area available for mass transfer. However, the increase in mass transfer rate coefficient is less pronounced in systems with larger solid particle radii due to the relatively smaller increase in specific interfacial area as the NAPL saturation increases. Alternatively, equation (29) can be used to examine the mass transfer rate coefficient as a function of saturation, contact angle, and fluid pore velocity. Figure 6b presents $\alpha$ as a function of $S_n$ for $R$=0.4, $v$ = 3.0 m/d and values of $\theta_c$ ranging from 15° to 50°. This figure shows that, as the contact angle increases at a particular value of $S_n$, the mass transfer rate coefficient decreases due to a decrease in interfacial area. Figure 6c shows $\alpha$ as a function of $S_n$ for $R$ = 0.4 mm, $\theta_c$ =30°, and $v$ = 1.0, 3.0, 10.0 m/d; this figure shows that, as the fluid pore velocity increases, the mass transfer rate coefficient increases due to the more rapid removal of solute from the interface between the NAPL and the aqueous phase.

The behavior of the mass transfer rate coefficient indicated in equation (32) is consistent with the power-function relationships commonly employed in the literature for dissolution from nonwetting NAPL distributed as spherical blobs in the pore bodies [*Miller et al.*, 1990; *Powers et al.*, 1992, 1994a; *Imhoff et al.*, 1994; *Bradford and Abriola*, 2001]. The predictive capability of the model for calculating the mass transfer rate coefficient as a function of the NAPL saturation and fluid velocity developed herein can be compared to that of empirical dissolution models which have appeared in the literature. Table 3 gives three correlations found in the literature [*Miller et al.*, 1990; *Imhoff et al.*, 1994; *Powers et al.*, 1994a]. Figure 7 compares the mass

**Table 3.** Empirical Correlations for Mass Transfer Rate Coefficients for NAPL Dissolution From Nonwetting Ganglia[a]

| Correlation | Reference |
|---|---|
| $\alpha = \frac{D_m}{d_{50}^2} 12 R_e^{0.75} S_n^{0.6} S_c^{0.5}$ | *Miller et al.* [1990] |
| $\alpha = \frac{D_m}{d_{50}^2} 340 R_e^{0.71} S_n^{0.87} (d_{50}/L)^{0.31}$ | *Imhoff et al.* [1994] |
| $\alpha = \frac{D_m}{d_{50}^2} 4.13 R_e^{0.598} \delta^{0.673} U_i^{0.369} (S_n/S_{ni})^{0.667}$ | *Powers et al.* [1994a] |

[a]Equations have been rewritten for consistency in notation. *Re* is the Reynolds number, defined as $Re = v\rho_w d_{50}/\mu_w$, where $v$ is the groundwater velocity (= 3.78 m/d) [*Powers et al.*, 1994a], $\rho_w$ and $\mu_w$ are the density and viscosity of water, respectively (= 998 kg/m$^3$ and $8.9 \times 10^{-4}$ N·s/m$^2$, respectively), and $d_{50}$ is median grain diameter (= 0.45 mm; Wagner 50 sand [*Powers et al.*, 1994a]). $S_c$ is the Schmitt number, defined as $S_c = \mu_w/(D_m\rho_w)$, where $D_m$ is the aqueous diffusion coefficient (= $8.8 \times 10^{-10}$ m$^2$/s; value for trichloroethylene from *Powers et al.* [1994a]). $L$ is the test column length (= 0.035 m; approximately average column length in *Powers et al.* [1994a]). $\delta$ is a normalized grain size, defined as $\delta = d_{50}/d_M$, where $d_M$ is the diameter of a medium sand grain (= 0. 5 mm), $U_i$ is the uniformity index (= 1.45; Wagner 50 sand [*Powers et al.*, 1994a]); $S_{ni}$ is the initial NAPL saturation (= 0.134) [*Powers et al.*, 1994a].

transfer rate coefficients calculated using the models presented in Table 3 with those calculated using the model proposed here. The *Miller et al.* [1990] model gives the largest values of $\alpha$. The *Powers et al.* [1994a] model gives smaller values of $\alpha$ than both our model and that of *Imhoff et al.* [1994], especially at higher NAPL saturations. The model developed here predicts faster mass transfer than the model of *Imhoff et al.* [1994] at low contact angles, though the prediction is similar at larger contact angles (e.g., $\theta_c = 70^\circ$). This observation is especially interesting since these empirical models were developed in systems where nonwetting NAPL blobs were distributed in the pore bodies, while the model developed here assumed a wetting NAPL phase, distributed as pendular rings at the soil contact points. Despite these widely different conceptualizations of the distribution of the residual NAPL, the dissolution predictions of the model developed here are within the range of those previously presented in the literature.

According to *Knutson et al.* [2001], whether there is a dependence of the mass transfer rate on NAPL configuration is contingent on the Peclet number, defined in that study as $Pe = vd/D_m$, where $d$ is the grain diameter. Taking $d = d_{50}$ and using the values from Table 3, $Pe = 22$ for the simulations shown in Figure 7. This value falls in the range of $Pe$ where, based on the work in *Knutson et al.* [2001], changes in the mass transfer rate coefficient are accounted for by variation in interfacial area, with only minor dependence on NAPL

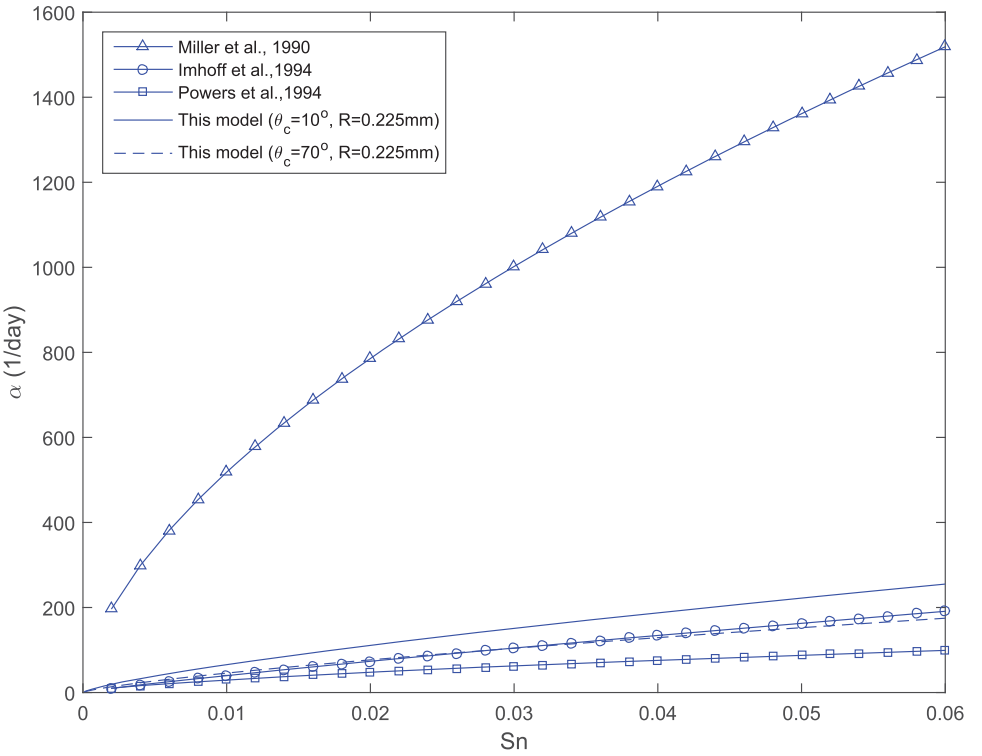


**Figure 7.** Comparison of the mass transfer rate coefficient $\alpha$ obtained by equation (29) and literature models given in Table 3.

configuration. The work presented here supports the conclusion that NAPL configuration is of lesser consequence at such values of *Pe*. Even the significant differences in the distribution of NAPL residual based on wettability, distributed either as blobs or as pendular rings, appear to be of secondary importance in calculating interfacial mass transfer under these conditions.

## 4. Conclusions

This work provides a theoretical means of calculating the rate of dissolution of NAPL in organic-wetting situations where the NAPL is immobilized as pendular rings surrounding the contact point between spherical soil particles. An exact solution to the Young-Laplace equation is presented assuming a hexagonal close packing of uniform solid spheres. The solution is presented in a novel form that yields an analytic $p_c$-$S_n$ relationship and facilitates the calculation of the pendular ring surface area and volume, enabling the quantification of the NAPL specific interfacial area and saturation. In addition, an exact solution to the advection-diffusion equation describing the transport of a solute in an equivalent capillary tube is presented, which, when coupled with the interfacial area, allows an analytic quantification of the mass transfer coefficient. Using these analytic expressions, a simple equation was obtained by regression to give the mass transfer rate coefficient as a function of the particle size ($R$), the contact angle ($\theta_c$), and the NAPL saturation ($S_n{}^n$), as well as a modified Peclet number ($Pe'$). Generally, correlations that have been developed to compute the mass transfer rate coefficient do not include the contact angle, whereas the model developed here does so explicitly. However, a comparison with empirically derived values for mass transfer rate coefficients in water-wet systems where the NAPL is distributed as blobs in pore bodies demonstrated that the values predicted here lie in the range of empirically derived values, despite the significant differences in system conceptualizations. Thus, this work implies that at higher values of *Pe*, differences in the rate of interfacial mass transfer can be accounted for by differences in interfacial area, and variability in the configuration of the NAPL residual between water-wet and organic-wet systems is of lesser importance.

## Appendix A: Derivation of the Mass Transfer Coefficient (Equation (22))

For relatively simple cases of well-defined geometries under ideal conditions, analytical expressions for the mass transfer coefficient describing NAPL dissolution can be derived. The porous medium can be conceptualized as a set of capillary tubes with an equivalent pore radius and a porosity of a hexagonal unit cell, with a stagnant layer of NAPL lining the inside of the tube (Figure A1). The water flows through the capillary tube in accordance with the Hagen-Poiseuille law, with mass transfer occurring across the NAPL-water interface. Assuming advection in the $x$ direction and diffusion in the $r$ direction, the steady state transport of the dissolved NAPL in the aqueous phase is governed by:

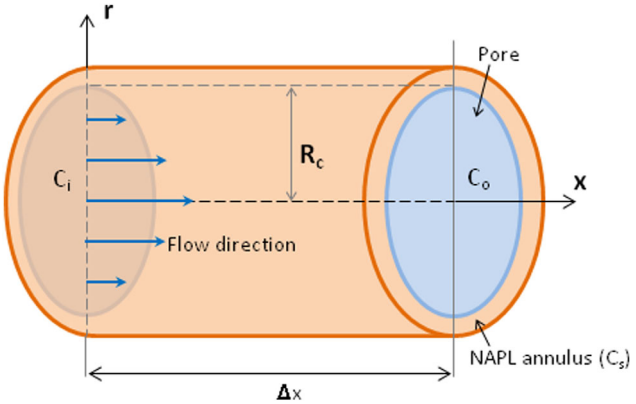


**Figure A1.** Capillary tube model for calculation of the mass transport coefficient. The capillary tube has an equivalent pore radius $R_c$, defined by equation (A3), and an inner surface covered by a stagnant layer of NAPL. Water flows through the tube in accordance with the Hagen-Poiseuille law and dissolution occurs at the surface of the NAPL annulus. The flow direction is aligned with the $x$ axis. The solute can advect in the $x$ direction and diffuse in the $r$ direction.

$$\frac{\partial}{\partial r}\left(rD_m\frac{\partial C}{\partial r}\right)-ru\frac{\partial C}{\partial x}=0 \qquad \text{(A1)}$$

where $C(x,r)$ is the aqueous-phase concentration of dissolved NAPL, $D_m$ is the molecular diffusion coefficient, $u$ is the velocity of pore fluid, $r$ is the coordinate in the radial direction of the capillary tube, and $x$ is the coordinate in the axial direction of the capillary tube. Based on the Hagen-Poiseuille law, the velocity of the pore fluid as a function of $r$ may be represented as [*Bear*, 1972]:

$$u=2v\left(1-\frac{r^2}{R_c^2}\right) \qquad \text{(A2)}$$

where $v$ is the average pore fluid velocity, $R_c$ is the equivalent pore radius, typically expressed as:

$$R_c = 2\theta / A_s \tag{A3}$$

where $\theta$ is the porosity, $A_s$ is the specific surface area of the solid particles, calculated as:

$$A_s = \frac{1}{20\sqrt{2}R}(48\Omega_T + 27\Omega_P) \tag{A4}$$

where $\Omega_T$ and $\Omega_P$ are the solid angles of a regular tetrahedron and square pyramid, respectively (see Table 1). The calculation of an arithmetic mean of the concentration:

$$\bar{C}(r) = \frac{1}{\Delta x}\int_0^{\Delta x} C(x, r)dx \tag{A5}$$

over a characteristic length $\Delta x$ in the direction of flow, calculated as the average pore volume $\bar{V}_p$, divided by the cross-sectional area of the capillary tube:

$$\Delta x = \frac{\bar{V}_p}{\pi R_c^2} \tag{A6}$$

where

$$\bar{V}_p = \frac{1}{21}(16\Omega_T + 9\Omega_P)R^3 \tag{A7}$$

simplifies the problem. Applying equation (A5) to equation (A1) yields:

$$\frac{d^2\bar{C}}{dr^2} + \frac{1}{r}\frac{d\bar{C}}{dr} - \beta(R_c^2 - r^2)\bar{C}_o = -\beta(R_c^2 - r^2)C_i \tag{A8}$$

where

$$\beta = \frac{2v}{D_m R_c^2 \Delta x} \tag{A9}$$

$C_i$ is the influent concentration of NAPL at $x = 0$, assumed constant over $r$ (except at $r = R_c$, where $C_i = C_s$), and equal to the concentration of dissolved NAPL in the bulk water entering the pore, $C_o(r)$ is the effluent concentration of dissolved NAPL leaving the pore, which equals $\bar{C}(r)$. Substituting $\bar{C}(r)$ for $C_o(r)$, equation (A8) can be rewritten as:

$$\frac{d^2\bar{C}}{dr^2} + \frac{1}{r}\frac{d\bar{C}}{dr} - \beta(R_c^2 - r^2)\bar{C} = -\beta(R_c^2 - r^2)C_i \tag{A10}$$

The boundary conditions for equation (A10) are:

$$\frac{\partial\bar{C}}{\partial r} = 0, \quad r = 0 \tag{A11}$$

$$\bar{C} = C_s, \quad r = R_c \tag{A12}$$

Using the following substitutions:

$$\bar{C} = \exp\left(-i\frac{1}{2}\sqrt{\beta}r^2\right)w(z) \tag{A13}$$

$$z = i\sqrt{\beta}r^2 \tag{A14}$$

the homogeneous counterpart of equation (A10) becomes:

$$z\frac{d^2w}{dz^2} + (b - z)\frac{dw}{dz} - aw = 0 \tag{A15}$$

where

$$a=\left(\frac{1}{2}-i\frac{1}{4}\sqrt{\beta}R_c^2\right) \tag{A16}$$

$$b=1 \tag{A17}$$

This is a confluent hypergeometric equation known as Kummer's equation and has the general solution:

$$w=AM(a,b,z)+BU(a,b,z) \tag{A18}$$

where $A$ and $B$ are the integration constants and $M(a,b,z)$ and $U(a,b,z)$ are the Kummer's functions. Substituting equation (A18) into equation (A13), we obtain the general solution for the homogeneous counterpart of equation (A10):

$$\bar{C}=\exp\left(-i\frac{1}{2}\sqrt{\beta}r^2\right)[A\,M(a,b,z)+B\,U(a,b,z)] \tag{A19}$$

Noting that $\bar{C}=C_i$ is a specific solution of equation (A10), the general solutions for equation (A10) is:

$$\bar{C}=\exp\left(-i\frac{1}{2}\sqrt{\beta}r^2\right)[A\,M(a,b,z)+B\,U(a,b,z)]+C_i \tag{A20}$$

Based on the boundary conditions (A11) and (A12), $B\equiv 0$ is required, and the final solution is:

$$\bar{C}=(C_s-C_i)\frac{\exp(-i\frac{1}{2}\sqrt{\beta}r^2)M(a,b,i\sqrt{\beta}r^2)}{\exp(-i\frac{1}{2}\sqrt{\beta}R_c^2)M(a,b,i\sqrt{\beta}R_c^2)}+C_i \tag{A21}$$

The mass flux $J_D$ across the NAPL-water interface becomes:

$$J_D=D_m\frac{d\bar{C}(R_c)}{dr}=D_m(C_s-C_i)\left[2a\frac{M(a+1,b+1,i\sqrt{\beta}R_c^2)}{M(a,b,i\sqrt{\beta}R_c^2)}-1\right]i\sqrt{\beta}R_c \tag{A22}$$

Using the definition of the mass transfer coefficient given in equation (29), equation (A22) leads to:

$$k_l=D_m\left[2a\frac{M(a+1,b+1,i\sqrt{\beta}R_c^2)}{M(a,b,i\sqrt{\beta}R_c^2)}-1\right]i\sqrt{\beta}R_c \tag{A23}$$

More conveniently, equation (A23) can be rewritten as:

$$k_l=\frac{D_m}{R_c}f(Pe') \tag{A24}$$

where

$$f(Pe')=\left[2a'\frac{M(a'+1,2,i\sqrt{Pe'})}{M(a',1,i\sqrt{Pe'})}-1\right]i\sqrt{Pe'} \tag{A25}$$

$$a'=\left(\frac{1}{2}-i\frac{1}{4}\sqrt{Pe'}\right) \tag{A26}$$

$$Pe'=\frac{2vR_c^2}{D_m\Delta x} \tag{A27}$$

$$R_c=\frac{40\sqrt{2}}{48\Omega_T+27\Omega_P}\theta R \tag{A28}$$

$$\Delta x=\frac{[60\sqrt{2}-3(16\Omega_T+9\Omega_P)](16\Omega_T+9\Omega_P)^2}{22400\pi}\frac{R}{\theta^2} \tag{A29}$$

where $Pe'$ is a modified Peclet number and $f(Pe')$ is a dimensionless function.

**Acknowledgments**
MATLAB® codes created for this analysis are available upon request by email: huang.junqi@epa.gov. Portions of this research were supported by the Strategic Environmental Research and Development Program (SERDP), project ER-1737. The authors are grateful for the constructive comments from the Editor and three anonymous reviewers. The content of this manuscript has not been subject to agency review and does not necessarily represent the view of the sponsoring agency. The views expressed in this manuscript are those of the authors and do not reflect the official policy or position of the United States Air Force, Department of Defense, or the U.S. Government.

## References

Bear, J. (1972), *Dynamics of Fluids in Porous Media*, Dover Publications, Inc., N. Y.
Bear, J., B. Rubinstein, and L. Fel (2011), Capillary pressure curve for liquid menisci in a cubic assembly of spherical particles below irreducible saturation, *Transp. Porous Media*, *89*, 63–73, doi:10.1007/s11242-011-9752-7.
Birak, P. S., and C. T. Miller (2009), Dense non-aqueous phase liquids at former manufactured gas plants: Challenges to modeling and remediation, *J. Contam. Hydrol.*, *105*, 81–98.
Bradford, S. A., and L. M. Abriola (2001), Dissolution of residual tetrachloroethylene in fractional wettability porous media: Incorporation of interfacial area estimates, *Water Resour. Res.*, *37*, 1183–1195.
Brusseau, M. L., S. Peng, G. Schnaar, and M. S. Costanza-Robinson (2006), Relationships among air-water interfacial area, capillary pressure, and water saturation for a sandy porous medium, *Water Resour. Res.*, *42*, W03501, doi:10.1029/2005WR004058.
Brusseau, M. L., H. Janousek, A. Murao, and G. Schnaar (2008), Synchrotron X-ray microtomography and interfacial partitioning tracer test measurements of NAPL-water interfacial areas, *Water Resour. Res.*, *44*, W01411, doi:10.1029/2006WR005517.
Cho, J., and M. D. Annable (2005), Characterization of pore scale NAPL morphology in homogeneous sands as a function of grain size and NAPL dissolution, *Chemosphere*, *61*, 899–908.
Christ, J., A. Ramsburg, L. Abriola, K. Pennell, and F. Loeffler, (2005), Coupling aggressive mass removal with microbial reductive chlorination for remediation of DNAPL source zones: A review and assessment, *Environ. Health Perspect.*, *113*(4), 465–474.
Culligan, K. A., D. Wildenschild, B. S. B. Christensen, W. G. Gray, M. L. Rivers, and A. F. B. Tompson (2004), Interfacial area measurements for unsaturated flow through a porous medium, *Water Resour. Res.*, *40*, W12413, doi:10.1029/2004WR003278.
Dobson, R., M. H. Schroth, M. Oostrom, and J. Zeyer (2006), Determination of NAPL-water interfacial areas in well-characterized porous media, *Environ. Sci. Technol.*, *40*, 815–822.
Dwarakanath, V., R. E. Jackson, and G. A. Pope (2002), Influence of wettability on the recovery of NAPLs from alluvium, *Environ. Sci. Technol.*, *36*, 227–231.
Grant, G. P., and J. I. Gerhard (2007), Simulating the dissolution of a complex dense nonaqueous phase liquid source zone: 1. Model to predict interfacial area, *Water Resour. Res.*, *43*, W12410, doi:10.1029/2007WR006038.
Gvirtzman, H., and P. V. Roberts (1991), Pore scale spatial analysis of two immiscible fluids in porous media, *Water Resour. Res.*, *27*, 1165–1176, doi:10.1029/91WR00303.
Hassanizadeh, S. M., and W. G. Gray (1993), Thermodynamic basis of capillary pressure in porous media, *Water Resour. Res.*, *29*, 3389–3405, doi:10.1029/93WR01495.
Held, R. J., and M. A. Celia (2001), Pore-scale modeling and upscaling of nonaqueous phase liquid mass transfer, *Water Resour. Res.*, *37*, 539–549, doi:10.1029/2000WR900274.
Hugaboom, D. A., and S. E. Powers (2002), Recovery of coal tar and creosote from porous media: The influence of wettability, *Ground Water Monit. Rem.*, *22*, 83–90.
Imhoff, P. T., P. R. Jaffé, and G. F. Pinder (1994), An experimental study of complete dissolution of a nonaqueous phase liquid in saturated porous media, *Water Resour. Res.*, *30*, 307–320, doi:10.1029/93WR02675.
Kueper, B. H., D. Redman, R. C. Starr, S. Reitsma, and M. Mah (1993), A field experiment to study the behavior of tetrachloroethylene below the water table: Spatial distribution of residual and pooled DNAPL, *Ground Water*, *31*, 756–766, doi:10.1111/j.1745-6584.1993.tb00848.x.
Knutson, C. E., C. J. Werth, and A. J. Valocchi (2001), Pore-scale modeling of dissolution from variably distributed nonaqueous phase liquid blobs, *Water Resour. Res.*, *37*, 2951–2963.
Leverett, M. C. (1941), Capillary behavior in porous solids, *Trans. Am. Inst. Min. Metall. Pet. Eng.*, *142*, 152–169.
Lord, D. L., K. F. Hayes, A. H. Demond, and A. Salehzadeh (1997a), Influence of organic acid solution chemistry on subsurface transport properties. 1. Surface and interfacial tension, *Environ. Sci. Technol.*, *31*, 2045–2051.
Lord, D. L., A. H. Demond, A. Salehzadeh, and K. F. Hayes (1997b), Influence of organic acid solution chemistry on subsurface transport properties. 2. Capillary pressure-saturation, *Environ. Sci. Technol.*, *31*, 2052–2058.
Melrose, J. C. (1966), Model calculations for capillary condensation, *AIChE J.*, *12*, 986–994.
Mercer, J. W., and R. M. Cohen (1990), A review of immiscible fluids in the subsurface: Properties, models, characterization, and remediation, *J. Contam. Hydrol.*, *6*, 107–163.
Miller, C. T., M. M. Poirier-McNeill, and A. S. Mayer (1990), Dissolution of trapped non-aqueous phase liquids: Mass transfer characteristics, *Water Resour. Res.*, *26*, 2783–2796.
Orr, F. M., L. E. Scriven, and A. P. Rivas (1975), Pendular rings between solids: Meniscus properties and capillary force, *J. Fluid Mech.*, *67*, 723–742.
Pearson, J. W. (2009), Computation of hypergeometric functions, MSc dissertation, Univ. of Oxford, Oxford, U. K. [Available at http://people.maths.ox.ac.uk/~porterm/research/pearson_final.pdf.]
Porter, M. L., D. Wildenschild, G. Grant, and J. I. Gerhard (2010), Measurement and prediction of the relationship between capillary pressure, saturation, and interfacial area in a NAPL-water-glass bead system, *Water Resour. Res.*, *46*, W08512, doi:10.1029/2009WR007786.
Powers, S. E., and M. E. Tamblin (1995), Wettability of porous media after exposure to synthetic gasolines, *J. Contam. Hydrol.*, *19*(2), 105–125.
Powers, S. E., L. M. Abriola, and W. J. Weber Jr. (1992), An experimental investigation of nonaqueous phase liquid dissolution in saturated subsurface systems: Steady-state mass transfer rates, *Water Resour. Res.*, *28*, 2691–2705.
Powers, S. E., L. M. Abriola, J. S. Dunkin, and W. J. Weber Jr. (1994a), Phenomenological model for transient NAPL-water mass transfer processes, *J. Contam. Hydrol.*, *16*, 1–33.
Powers, S. E., L. M. Abriola, and W. J. Weber Jr. (1994b), An experimental investigation of nonaqueous phase liquid dissolution in saturated subsurface systems: Transient mass transfer rates, *Water Resour. Res.*, *30*, 321–332.
Reeves, P. C., and M. A. Celia (1996), A functional relationship between capillary pressure, saturation, and interfacial area as revealed by a pore-scale network model, *Water Resour. Res.*, *32*, 2345–2358, doi:10.1029/96WR01105.
Rey, A. D. (2000), Young-Laplace equation for liquid crystal interfaces, *J. Chem. Phys.*, *113*, 10,820–10,822.
Rubinstein, B. Y., and L. G. Fel (2013), Theory of axisymmetric pendular rings, *J. Colloid Interface Sci.*, *417*, 37–50, doi:10.1016/j.jcis.2013.11.038.
Ryder, J. L., and A. H. Demond (2008), Wettability hysteresis and its implications for DNAPL source zone distribution, *J. Contam. Hydrol.*, *102*, 39–48.
US EPA (2003), The DNAPL remediation challenge: Is there a case for source depletion?, *Rep. EPA/600/R-03/143*, Office of Research and Development, Cincinnati, Ohio.
Weber, W. J., Jr., and F. A. DiGiano (1996), *Process Dynamics in Environmental Systems*, John Wiley, N. Y.
Young, C. M., R. E. Jackson, M. Jin, J. T. Londergan, P. E. Mariner, G. A. Pope, F. J. Anderson, and T. Houk (1999), Characterization of a TCE DNAPL zone in alluvium by partitioning tracers, *Ground Water Monit. Rem.*, *19*(1), 84–94.
Zheng, J., and S. E. Powers (1999), Organic bases in NAPLs and their impact on wettability, *J. Contam. Hydrol.*, *39*, 161–181.